

Journal of
Mechanics of
Materials and Structures

**ASYMPTOTIC ANALYSIS AND REFLECTION PHOTOELASTICITY
FOR THE STUDY OF TRANSIENT CRACK PROPAGATION IN
GRADED MATERIALS**

Nitesh Jain and Arun Shukla

Volume 2, N° 4

April 2007

ASYMPTOTIC ANALYSIS AND REFLECTION PHOTOELASTICITY FOR THE STUDY OF TRANSIENT CRACK PROPAGATION IN GRADED MATERIALS

NITESH JAIN AND ARUN SHUKLA

The behavior of a rapidly moving transient crack in functionally graded materials (FGMs) is investigated theoretically and experimentally. First, a systematic theoretical analysis is presented for the development of the transient elastodynamic local stress, strain, and displacement field expansions near a growing mixed mode crack tip in FGMs. The crack propagation direction is assumed to be inclined to the direction of the property variation. The displacement potential approach in conjunction with asymptotic analysis is utilized to derive explicit expressions for stress, strain, and in-plane displacement fields. The transient crack growth is assumed to include processes in which both the crack tip speed and the dynamic stress intensity factor are differentiable functions of time. These stress fields are used to generate the contours of constant maximum shear stress (isochromatics fringes) and the effect of transient crack growth on these contours is discussed. To further understand the transient crack growth behavior, a series of dynamic fracture experiments are performed with functionally graded material fabricated in-house. The phenomenon of transition from a static crack to a dynamic mode I crack is examined in these experiments. The full-field stress data around the crack is recorded using dynamic photoelasticity and high-speed digital photography. Due to opaqueness of FGMs, birefringent coatings are employed to obtain the full-field isochromatics around the crack tip. The stress field expansions developed in the first part of the study are used to interpret the experimental observations. The results of the experiments showed that the higher order transient expansion provides an accurate representation of crack tip fields under severe transient conditions.

1. Introduction

Increasing multifunctional performance requirements in aerospace, power generation, microelectronics, and bioengineering applications often demand properties that are unattainable with any single material. Correspondingly, composite and layered materials are developed to invoke the desirable characteristic of each constituent phase in order to meet such requirements. However, the internal stresses caused by the elastic and the thermal property mismatch at an interface between two differing bulk materials can mitigate the successful implementation of such composites. To address this problem, functionally gradient materials (FGMs) have been developed. FGMs accommodate a gradual transition of the properties of different materials from one location to the other, such that the mismatch in mechanical and thermal properties is minimized [Surendranath et al. 2003; Suresh and Mortensen 1998].

Keywords: functionally graded material, dynamic fracture, transient crack, asymptotic analysis, photoelasticity, high-speed imaging.

This work was supported by the National Science Foundation under grant CMS-0244330 and by the Air Force Office of Scientific Research under grant FA-95500610162.

A fundamental understanding of the mechanics of crack formation, initiation, and growth is essential for efficient design of critical components fabricated using FGMs. Several researchers have investigated the behavior of embedded and edge cracks in graded materials subjected to quasistatic loading [Jin and Noda 1994; Erdogan 1995; Gu and Asaro 1997; Chalivendra et al. 2003; Jain et al. 2004]. All these studies concluded that the inverse square-root singularity at the crack tip is not affected by material nonhomogeneities as long as the elastic modulus and Poisson's ratio are sufficiently smooth functions of spatial position. Although the stationary crack problem in FGMs has received considerable attention, less is known about the behavior of a rapidly propagating crack in these materials. The problem of a crack moving with a constant velocity in FGMs has been presented by [Atkinson and List 1978; Wang and Meguid 1994; Nakagaki et al. 1998; Parameswaran and Shukla 1998; Marur and Tippur 2000; Rousseau and Tippur 2001; Li and Weng 2002; Jain and Shukla 2004; Jain and Shukla 2006]. Recently, there has been some work on the fracture mechanics of anisotropic functionally graded materials. Sladek et al. [2005] proposed a meshless method based on the local Petrov–Galerkin approach for crack analysis in anisotropic FGMs. Kim and Paulino [2004] presented an interaction integral formulation for evaluating the elastic T-stress for a mixed mode crack in orthotropic nonhomogeneous materials. In most of these investigations, it is presumed that the crack tip stress field depends upon the instantaneous crack velocity and the instantaneous stress intensity factor. However, in many situations, reflecting stress waves pass through the specimen constructively and destructively interfering with one another, and thus result in a highly complex time-dependent stress intensity factor. Due to the nonhomogeneous nature of FGM and resulting mathematical complexities, very few investigations on the transient dynamic response of cracked FGMs have been reported in the literature [Zhang et al. 2003; Shukla and Jain 2004; Chalivendra et al. 2003]. In all these investigations the crack is subjected to a single mode of loading, that is, either an opening or a tearing mode. But from a practical viewpoint, strength-controlling flaws in load bearing structures, in general, are expected to be inclined at random orientations to the applied principal stress. Also, it has been reported in experimental and numerical studies that propagating cracks in FGMs can follow inclined paths under various loading conditions due to spatial variation of properties in graded materials [Li et al. 2000; Tilbrook et al. 2005; Abanto-Bueno and Lambros 2006]. The transient elastodynamic solution for a crack growing in an arbitrary direction in FGMs is still not known. However, the solution for a homogeneous material is presented in the work of [Freund and Rosakis 1992].

This paper provides a theoretical analysis for the derivation of transient, asymptotic, elastodynamic near-tip fields for a crack growing in an arbitrary direction in an FGM. The transient elastodynamic problem is formulated in terms of two displacement potentials, and an asymptotic analysis is performed to develop explicit expressions for stress, strain, and in-plane displacement fields. In this context, transient crack growth is understood to include processes in which both the crack tip speed and the dynamic stress intensity factor are differentiable functions of time. These crack tip fields are needed to analyze the full-field experimental data obtained from various experimental techniques such as photoelasticity, Moiré interferometry, holographic interferometry, and coherent gradient sensing (CGS). The stress fields developed in this paper are used to generate the contours of constant maximum shear stress (isochromatic fringes) and the effect of the transient crack growth on these contours is discussed. This is followed by a series of experiments to get further insight into the behavior of mode-I transient cracks in FGMs. The full-field stress data around the propagating crack is recorded using dynamic photoelasticity and high speed digital photography. Due to the opaqueness of FGMs, birefringent coatings are employed to obtain

the full-field isochromatic fringes around the moving crack tip. A high speed camera capable of taking 200 million frames per second is used to record these isochromatic fringes. The stress field expansion developed in the first part of the study is used to interpret these experimental observations, with the conclusion that the higher order expansion provides an accurate representation of crack tip fields under severe transient conditions.

2. Elastodynamic transient crack tip fields

2.1. Theoretical consideration. The variation of elastic and physical properties in FGMs is in general limited to a single direction. At any given point in the material, the properties can be assumed to be the same in all directions and hence, at a continuum level FGMs are isotropic nonhomogeneous solids. The transient elastodynamic problem is formulated in terms of two displacement potentials and an asymptotic analysis is performed to develop the stress, strain, and displacement fields around a propagating crack in an FGM. The direction of transient crack propagation is assumed to be inclined to the direction of property variation. The properties are assumed to vary exponentially with distance. When the crack is inclined to the property gradation direction, the stress state near the crack tip is mixed mode, irrespective of the far field loading.

2.2. Theoretical formulation. Consider a crack moving nonuniformly in an FGM as shown in Figure 1. The original coordinate system is a spatially fixed Cartesian coordinate system $X - Y$. A moving coordinate system $x - y$ at the crack tip is now defined such that the crack velocity is in the x -direction. Suppose that the crack propagates with a nonuniform speed, $c(t)$, and the crack faces satisfy the traction free boundary condition. Localized crack tip plasticity and three-dimensional effects are neglected in this formulation. The shear modulus and mass density are assumed to vary exponentially in the X_1 direction as given in (1) and the Poisson's ratio ν is assumed to be constant. The property gradation direction forms an angle φ with the $Y = 0$ axis. We have

$$\mu = \mu_0 \exp(\delta X_1), \quad \rho = \rho_0 \exp(\delta X_1), \quad S = \frac{\lambda}{\mu}, \tag{1}$$

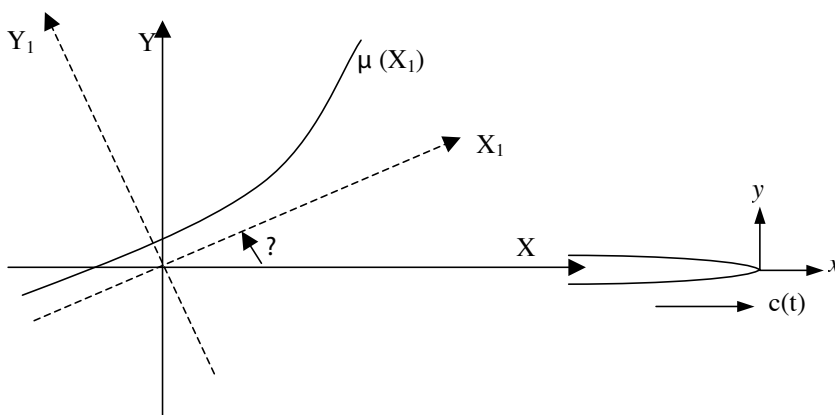


Figure 1. Propagating crack orientation with respect to the direction of property variation in a FGM.

where μ and λ are the shear modulus and Lamé’s constant, μ_0 and ρ_0 are the shear modulus and mass density at $X = X_1 = 0$, and δ is the nonhomogeneity parameter, having the dimension of inverse length. Equation (1) can be written in terms of (X, Y) coordinates by using a simple transformation

$$\begin{aligned} \mu(X, Y) &= \mu_0 \exp(\alpha X + \beta Y), & \rho(X, Y) &= \rho_0 \exp(\alpha X + \beta Y), & (2) \\ \alpha &= \delta \cos \varphi, & \beta &= \delta \sin \varphi. & (3) \end{aligned}$$

The equations of motion for a plane problem in the absence of body forces in the fixed coordinate system can be written as

$$\sigma_{XX,X} + \sigma_{XY,Y} = \rho u_{,tt}, \quad \sigma_{XY,X} + \sigma_{YY,Y} = \rho v_{,tt}, \quad (4)$$

where σ_{ij} are in-plane stress components and u, v are in-plane displacements. The Hooke’s law for plane elasticity problem can be written as

$$\begin{aligned} \sigma_{XX} &= ((\lambda_0 + 2\mu_0)u_{,X} + \lambda_0 v_{,Y}) \exp(\alpha X + \beta Y), \\ \sigma_{YY} &= ((\lambda_0 + 2\mu_0)v_{,Y} + \lambda_0 u_{,X}) \exp(\alpha X + \beta Y), & (5) \\ \sigma_{XY} &= (u_{,Y} + v_{,X})\mu_0 \exp(\alpha X + \beta Y). \end{aligned}$$

Introducing the displacement potentials (Φ and Ψ) as

$$u = \Phi_{,X} + \Psi_{,Y}, \quad v = \Phi_{,Y} - \Psi_{,X}, \quad (6)$$

substituting (6) into (5), and substituting the resulting equality into (4), the equation of motion can be expressed in terms of displacement potentials Φ and Ψ as

$$\begin{aligned} \frac{\partial}{\partial X} \left((S + 2)\nabla^2 \Phi - \frac{\rho_0}{\mu_0} \frac{\partial^2 \Phi}{\partial t^2} \right) + \frac{\partial}{\partial Y} \left(\nabla^2 \Psi - \frac{\rho_0}{\mu_0} \frac{\partial^2 \Psi}{\partial t^2} \right) \\ + \alpha \left(S\nabla^2 \Phi + 2\frac{\partial^2 \Phi}{\partial X^2} + 2\frac{\partial^2 \Psi}{\partial X \partial Y} \right) + \beta \left(2\frac{\partial^2 \Phi}{\partial X \partial Y} + \frac{\partial^2 \Psi}{\partial Y^2} - \frac{\partial^2 \Psi}{\partial X^2} \right) = 0, \\ \frac{\partial}{\partial Y} \left((S + 2)\nabla^2 \Phi - \frac{\rho_0}{\mu_0} \frac{\partial^2 \Phi}{\partial t^2} \right) - \frac{\partial}{\partial X} \left(\nabla^2 \Psi - \frac{\rho_0}{\mu_0} \frac{\partial^2 \Psi}{\partial t^2} \right) \\ + \alpha \left(\frac{\partial^2 \Psi}{\partial Y^2} - \frac{\partial^2 \Psi}{\partial X^2} + 2\frac{\partial^2 \Phi}{\partial X \partial Y} \right) + \beta \left((S + 2)\frac{\partial^2 \Phi}{\partial Y^2} - 2\frac{\partial^2 \Psi}{\partial X \partial Y} + \lambda_0 \frac{\partial^2 \Phi}{\partial X^2} \right) = 0. \end{aligned} \quad (7)$$

Equations (7) can only be satisfied when (see [Jain and Shukla 2004])

$$\begin{aligned} (S + 2)\nabla^2 \Phi - \frac{\rho_0}{\mu_0} \frac{\partial^2 \Phi}{\partial t^2} + (S + 2)\left(\alpha \frac{\partial \Phi}{\partial X} + \beta \frac{\partial \Phi}{\partial Y}\right) + \left(\alpha \frac{\partial \Psi}{\partial Y} - \beta \frac{\partial \Psi}{\partial X}\right) = 0, & (8) \\ \nabla^2 \Psi - \frac{\rho_0}{\mu_0} \frac{\partial^2 \Psi}{\partial t^2} + S\left(\alpha \frac{\partial \Phi}{\partial Y} - \beta \frac{\partial \Phi}{\partial X}\right) + \left(\alpha \frac{\partial \Psi}{\partial X} + \beta \frac{\partial \Psi}{\partial Y}\right) = 0. \end{aligned}$$

Now we introduce the moving crack tip coordinates $x = X - ct$ and $y = Y$. The coordinate change implies the substitutions

$$\frac{\partial^2}{\partial X^2} = \frac{\partial^2}{\partial x^2} \quad \text{and} \quad \frac{\partial^2}{\partial t^2} = c^2 \frac{\partial^2}{\partial x^2} + \frac{\partial^2}{\partial t^2} - \dot{c} \frac{\partial}{\partial x} - 2c \frac{\partial^2}{\partial x \partial t}, \quad \text{where } \dot{c} = \frac{\partial c}{\partial t}. \quad (9)$$

Using these transformations, Equation (8) becomes

$$\alpha_l^2 \frac{\partial^2 \Phi}{\partial x^2} + \frac{\partial^2 \Phi}{\partial y^2} + \left(\alpha \frac{\partial \Phi}{\partial x} + \beta \frac{\partial \Phi}{\partial y} \right) - \frac{1}{S+2} \left(\alpha \frac{\partial \Psi}{\partial y} - \beta \frac{\partial \Psi}{\partial x} \right) + \frac{\rho_0}{\mu_0(S+2)} \left(\dot{c} \frac{\partial \Phi}{\partial x} + 2c \frac{\partial^2 \Phi}{\partial x \partial t} - \frac{\partial^2 \Phi}{\partial t^2} \right) = 0,$$

$$\alpha_s^2 \frac{\partial^2 \Psi}{\partial x^2} + \frac{\partial^2 \Psi}{\partial y^2} + \left(\alpha \frac{\partial \Psi}{\partial x} + \beta \frac{\partial \Psi}{\partial y} \right) + S \left(\alpha \frac{\partial \Phi}{\partial y} - \beta \frac{\partial \Phi}{\partial x} \right) + \frac{\rho_0}{\mu_0(S+2)} \left(\dot{c} \frac{\partial \Psi}{\partial x} + 2c \frac{\partial^2 \Psi}{\partial x \partial t} - \frac{\partial^2 \Psi}{\partial t^2} \right) = 0, \tag{10}$$

where

$$\alpha_l = \left(1 - \frac{\rho_0 c^2}{\mu_0(S+2)} \right)^{1/2}, \quad \alpha_s = \left(1 - \frac{\rho_0 c^2}{\mu_0} \right)^{1/2}.$$

These equations reduce to the classical two-dimensional wave equations of motion if α and β equal zero. In the case of nonhomogeneity, the equations lose their classical form and remain coupled in Φ and Ψ , through the nonhomogeneity parameters α and β .

2.3. Asymptotic expansion of crack tip fields. At this point, we employ the standard asymptotic analysis proposed in [Freund 1990]. We introduce coordinates $\eta_1 = x/\varepsilon$, $\eta_2 = y/\varepsilon$, where ε is a small arbitrary positive parameter ($0 < \varepsilon < 1$), used so that the region around the crack tip is expanded to fill the entire region of observation. As ε becomes infinitely small, all the points in the x - y plane, except those very near the crack tip, are pushed out of the field of observation in the η_1 - η_2 plane, and the crack line occupies the whole negative η_1 -axis. We assume that Φ and Ψ can be expressed in powers of ε as

$$\Phi(x, y) = \Phi(\varepsilon\eta_1, \varepsilon\eta_2) = \sum_{m=0}^{\infty} \varepsilon^{(m+3)/2} \phi_m(\eta_1, \eta_2),$$

$$\Psi(x, y) = \Psi(\varepsilon\eta_1, \varepsilon\eta_2) = \sum_{m=0}^{\infty} \varepsilon^{(m+3)/2} \psi_m(\eta_1, \eta_2). \tag{11}$$

The first term of series ($m = 0$) corresponds to the expected square root singular contribution proportional to $r^{-1/2}$ in the asymptotic near-tip stress field.

Substituting the assumed asymptotic form (11) into the governing Equation (10), we obtain two equations, in each of which the left-hand side is an infinite power series in ε and the right-hand side vanishes. Since ε is an arbitrary number, the coefficient of each power of ε should vanish identically to satisfy these resulting equations. Therefore, the governing equation reduces to a system of coupled differential equations in Φ and Ψ . These equations have the general form

$$\alpha_l^2 \frac{\partial^2 \phi_m}{\partial \eta_1^2} + \frac{\partial^2 \phi_m}{\partial \eta_2^2} + \left(\alpha \frac{\partial \phi_{m-2}}{\partial \eta_1} + \beta \frac{\partial \phi_{m-2}}{\partial \eta_2} \right) + \frac{1}{S+2} \left(\alpha \frac{\partial \psi_{m-2}}{\partial \eta_2} - \beta \frac{\partial \psi_{m-2}}{\partial \eta_1} \right)$$

$$+ \frac{\rho_0 c^{1/2}}{\mu_0(S+2)} \frac{\partial}{\partial t} \left(c^{1/2} \frac{\partial \phi_{m-2}}{\partial \eta_1} \right) - \frac{\rho_0}{\mu_0(S+2)} \frac{\partial^2 \phi_{m-4}}{\partial t^2} = 0,$$

$$\alpha_s^2 \frac{\partial^2 \psi_m}{\partial \eta_1^2} + \frac{\partial^2 \psi_m}{\partial \eta_2^2} + \left(\alpha \frac{\partial \psi_{m-2}}{\partial \eta_1} + \beta \frac{\partial \psi_{m-2}}{\partial \eta_2} \right) + S \left(\alpha \frac{\partial \phi_{m-2}}{\partial \eta_2} - \beta \frac{\partial \phi_{m-2}}{\partial \eta_1} \right)$$

$$+ \frac{\rho_0 c^{1/2}}{\mu_0} \frac{\partial}{\partial t} \left(c^{1/2} \frac{\partial \psi_{m-2}}{\partial \eta_1} \right) - \frac{\rho_0}{\mu_0(S+2)} \frac{\partial^2 \psi_{m-4}}{\partial t^2} = 0, \tag{12}$$

where

$$\phi_k, \psi_k = \begin{cases} \phi_k, \psi_k & \text{for } k \geq 0, \\ 0 & \text{for } k < 0. \end{cases}$$

For $m = 0$ and $m = 1$, Equations (12) are not coupled in Φ and Ψ and reduce to Laplace’s equation in the coordinates $\eta_1, \alpha_l \eta_2$ or $\eta_1, \alpha_s \eta_2$ (similar to that for a homogeneous material having elastic properties equal to the elastic properties of the FGM at the crack tip). Indeed, as will be seen, ϕ_0 and ψ_0 have the same spatial structure in both transient and steady state cases. This is not so, however, for ϕ_m, ψ_m if $m > 1$.

Since the crack is propagating at an angle to the direction of property gradation, the stress field near the crack tip is a combination of both opening and shear modes (mixed mode). For the elastic solution, the stress field related to the opening mode and the shear modes can be superposed to obtain the mixed mode solution. The solutions for $m = 0$ and 1 are the same as for homogeneous material and can be written as

$$\begin{aligned} \phi_m(\rho_l, \theta_l, t) &= A_m(t)\rho_l^{(m+3)/2} \cos \frac{1}{2}(m+3)\theta_l + C_m(t)\rho_l^{(m+3)/2} \sin \frac{1}{2}(m+3)\theta_l, \\ \psi_m(\rho_s, \theta_s, t) &= B_m(t)\rho_s^{(m+3)/2} \sin \frac{1}{2}(m+3)\theta_s + D_m(t)\rho_s^{(m+3)/2} \cos \frac{1}{2}(m+3)\theta_s \end{aligned} \tag{13}$$

for $m = 0, 1$, where

$$\rho_l = (\eta_1^2 + \alpha_l^2 \eta_2^2)^{1/2}, \quad \tan \theta_l = \frac{\alpha_l \eta_2}{\eta_1}, \quad \rho_s = (\eta_1^2 + \alpha_s^2 \eta_2^2)^{1/2}, \quad \tan \theta_s = \frac{\alpha_s \eta_2}{\eta_1}.$$

The solution (13) appears to be the same as for steady state crack growth. However, the two solutions differ fundamentally in that the coordinates (ρ_l, θ_l) now depend upon time. It is the crack speed that determines the degree of distortion of these coordinates, and the crack speed is now a function of time. Also one should note that the coefficients of the series solution given in (13) are time dependent.

Using the definitions of dynamic stress intensity factors K_{ID} and K_{IID} for the opening and the shear modes [Shukla and Chona 1987] and considering the crack face boundary conditions we get

$$\begin{aligned} A_0(t) &= \frac{4(1 + \alpha_s^2)}{3(4\alpha_s \alpha_l - (1 + \alpha_s^2)^2)} \frac{K_{ID}(t)}{\mu_c \sqrt{2\pi}}, & B_0(t) &= -\frac{2\alpha_l}{1 + \alpha_s^2} A_0(t), \\ C_0(t) &= \frac{8\alpha_s}{3(4\alpha_s \alpha_l - (1 + \alpha_s^2)^2)} \frac{K_{IID}(t)}{\mu_c \sqrt{2\pi}}, & D_0(t) &= \frac{1 + \alpha_s^2}{2\alpha_l} C_0(t). \end{aligned} \tag{14}$$

The solution for higher orders of m can be obtained recursively (see [Jain and Shukla 2004]):

$$\begin{aligned} \phi_2 &= A_2(t)\rho_l^{5/2} \cos \frac{5}{2}\theta_l - \frac{1}{4}\alpha_l^{-2}\rho_l^{5/2}(\cos \frac{1}{2}\theta_l(\alpha A_0(t) + \beta C_0(t)) + \sin \frac{1}{2}\theta_l(\alpha C_0(t) - \beta A_0(t))) \\ &\quad - \frac{2}{5} \frac{\alpha_s}{(k+2)(\alpha_l^2 - \alpha_s^2)} \rho_s^{5/2}(\cos \frac{5}{2}\theta_s(\alpha B_0(t) - \beta D_0(t)) - \sin \frac{5}{2}\theta_s(\alpha B_0(t) + \beta D_0(t))) \\ &\quad + \rho_l^{5/2} \left(\frac{1}{6}(D_l(A_0(t)) + \frac{1}{2}B_l^A(t)) \cos \frac{1}{2}\theta_l - \frac{1}{8}B_l^A(t) \cos \frac{3}{2}\theta_l \right. \\ &\quad \left. + \frac{1}{6}(D_l(C_0(t)) + \frac{1}{2}B_l^C(t)) \sin \frac{1}{2}\theta_l + \frac{1}{8}B_l^C(t) \sin \frac{3}{2}\theta_l \right), \end{aligned}$$

$$\begin{aligned} \psi_2 = & B_2(t)\rho_s^{5/2} \sin \frac{5}{2}\theta_s - \frac{1}{4}\alpha_s^{-2}\rho_s^{5/2}(\cos \frac{1}{2}\theta_s(\alpha B_0(t) + \beta D_0(t)) + \sin \frac{1}{2}\theta_s(\alpha B_0(t) - \beta D_0(t))) \\ & + \frac{2}{5} \frac{k\alpha_l}{(\alpha_l^2 - \alpha_s^2)}\rho_l^{5/2}(\cos \frac{5}{2}\theta_l(\alpha C_0(t) - \beta A_0(t)) - \sin \frac{5}{2}\theta_l(\alpha A_0(t) + \beta C_0(t))) \\ & + \rho_s^{5/2}\left(\frac{1}{6}(D_s(B_0(t)) + \frac{1}{2}B_s^B(t)) \sin \frac{1}{2}\theta_s + \frac{1}{8}B_s^B(t) \sin \frac{3}{2}\theta_s \right. \\ & \left. + \frac{1}{6}(D_s(D_0(t)) + \frac{1}{2}B_s^D(t)) \cos \frac{1}{2}\theta_s - \frac{1}{8}B_s^D(t) \cos \frac{3}{2}\theta_s\right). \quad (15) \end{aligned}$$

The coefficients appearing in this solution are defined in the Appendix.

2.4. Stress, strain, and displacement fields. The stress, strain, and displacement fields around the crack tip can now be obtained using displacement potentials (Φ and Ψ) found in the previous section. Detailed expressions for the stress, strain, and displacements are not included here for brevity, but they are provided in an online supplement to this paper. The authors can supply these expressions in machine readable form upon request.

2.5. Discussions of solutions. To get an insight into the effects of transient terms on the dynamic fracture process, contours of constant maximum shear stress (isochromatics) and contours of constant first stress invariant (isopachics) are generated for mixed mode loading conditions. The asymptotic representation of crack tip stress and displacement fields contain coefficients $A_n(t)$, $B_n(t)$, $C_n(t)$, and $D_n(t)$, which can be related to fracture parameters such as stress intensity factor and nonsingular stress components as in (14). The contours are generated for assumed values of the dynamic stress intensity factors (coefficient A_0 and C_0), whereas the higher order coefficients A_1 , A_2 , C_1 , C_2 , B_1 , B_2 , D_1 and D_2 are assumed to be zero. However, the nonhomogeneity and transient specific parts of the higher order terms, that have A_0 , B_0 , C_0 and D_0 as the coefficients, are retained. The typical values of material properties and material thickness used in generating contours are as follows: Poisson’s ratio = 0.3, shear modulus at the crack tip $\mu_c = 1.5$ GPa, density at the crack tip $\rho_c = 1200$ kg/m³, and thickness $t = 0.01$ m. The nonhomogeneity parameter α for plotting these contours is obtained by fitting an exponential curve to the property variation profile of the laboratory-fabricated FGMs [Jain and Shukla 2006]. The nonhomogeneity parameter α for FGM fabricated in this study is 0.57. The crack velocity used in generating all the contours is 650 ms⁻¹. This choice of velocity is made on the basis of available experimental data on velocities that are typically observed for this FGM [Jain and Shukla 2006].

2.5.1. Isochromatic fringe patterns. Isochromatic fringe patterns obtained in photoelasticity represent contours of constant maximum shear stress and their generation is governed by the stress-optic law

$$\frac{Nf_\sigma}{2h} = \tau_{\max} = \frac{\sigma_1 - \sigma_2}{2} = \sqrt{\left(\frac{\sigma_x - \sigma_y}{2}\right)^2 + \tau_{xy}^2}, \quad (16)$$

where f_σ is the material fringe value, N is the isochromatic fringe order and h is the thickness of the specimen. Equation (16) is used to generate the isochromatic fringe patterns around the crack tip in FGMs. In generating these contours the crack is assumed to be on the negative x -axis and the crack tip is located at (0, 0). Also, the direction of crack propagation is assumed to be towards the positive x -axis. Figure 2 shows the effect of the rate of change of mode- I stress intensity factor ($dK_{ID}(t)/dt$) on contours of constant maximum shear stress for mixed mode loading around the crack tip corresponding

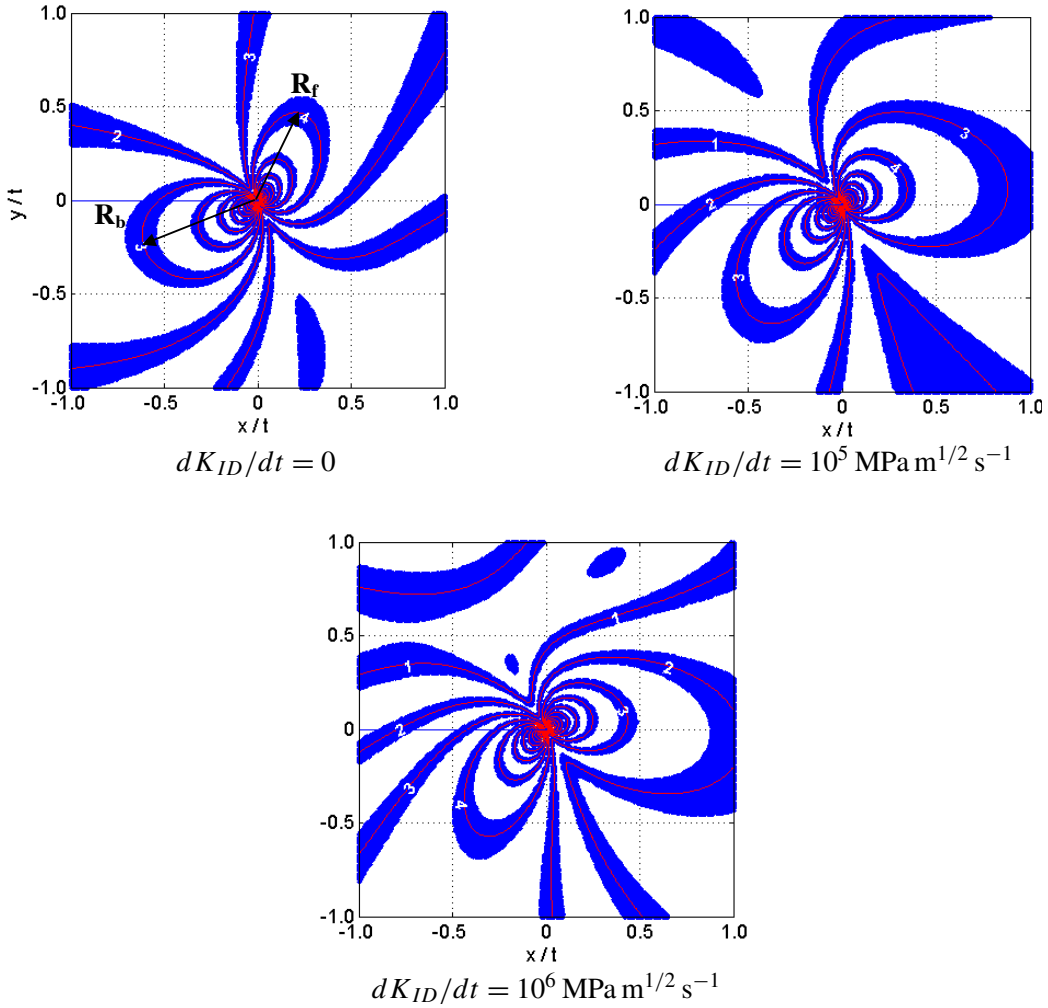


Figure 2. Effect of the rate of change of mode-I stress intensity factor on the contours of constant maximum shear stress around the crack tip in an FGM ($\alpha = 0.57$, $K_{ID}(t) = 1 \text{ MPa m}^{1/2}$, $K_{IID}(t) = 1 \text{ MPa m}^{1/2}$, $c = 650 \text{ ms}^{-1}$, $dc/dt = 0$). The front and rear apogee radii are marked in part (a) with R_f and R_b , respectively.

to $\alpha = 0.57$, $K_{ID} = K_{IID} = 1.0 \text{ MPa m}^{1/2}$, and $c = 650 \text{ ms}^{-1}$. As observed in [Dally and Shukla 1979] the rate of change of K_{ID} at crack initiation could be of the order of $10^5 \text{ MPa m}^{1/2} \text{ sec}^{-1}$, the values of $dK_{ID}(t)/dt$ are varied over six orders of magnitude for generating the contours. The fringe order increases as the crack tip is approached, with very high fringe orders in the close vicinity of the crack tip. This is a direct consequence of the stress singularity that exists at the crack tip. As $dK_{ID}(t)/dt$ increases, the fringes in front of the crack tip decrease in size and number, and the reverse happens for fringes behind the crack tip. This effect can be quantified in terms of increase in apogee radius (see Figure 2a) of a given fringe.

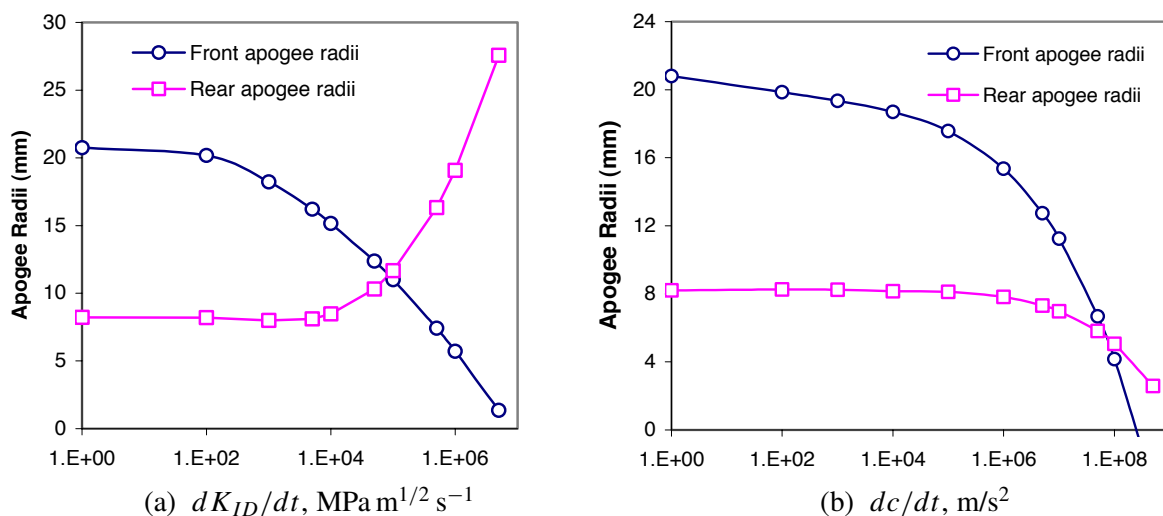


Figure 3. Variation of apogee radii of the third order isochromatic fringe as a function of (a) rate of change of mode-I stress intensity factor, and (b) crack tip acceleration.

The front and rear apogee radii of the third fringe order are determined from isochromatic fringe patterns and are plotted in Figure 3a as functions of $dK_{ID}(t)/dt$. The front apogee radius decreases from 20.7 mm to 5.7 mm as $dK_{ID}(t)/dt$ increases from 0 to $10^6 \text{ MPa m}^{1/2} \text{ s}^{-1}$. The corresponding increase in the rear apogee radius is from 8.2 mm to 19.1 mm. The dependence of the fringe radius on the rate of change of mode-I stress intensity factor is nonlinear; a rapid change in the front and rear apogee radii are observed at higher values of $dK_{ID}(t)/dt$.

An additional consequence of the variation of the rate of change of mode I stress intensity factor is its effect on the tilt and shape of the isochromatic fringe contours surrounding the crack tip, as observed in Figure 2. As $dK_{ID}(t)/dt$ increases the fringes on the front side of the crack tip bend towards the direction of crack propagation and the fringes on the rear side bend away from the crack faces.

Figure 3b and Figure 4 show data obtained for a crack propagating in an FGM under different values of crack acceleration. The value of dc/dt is varied over eight orders of magnitude. (Dally and Shukla [1979] showed that the rate of change of velocity at crack initiation could be of the order of 10^7 ms^{-2} in their work with homogeneous materials.) Figure 4 shows isochromatic fringes for $dc/dt = 10^6, 10^7$ and 10^8 ms^{-2} . The changes in fringe size and shape until crack tip accelerations of 10^6 ms^{-2} are reached are negligible. For dc/dt above 10^6 ms^{-2} , as the crack acceleration increases, the front and rear fringe loops decrease in size. Figure 3b shows the variation of the front and the rear apogee radii of the third order fringe as a function of crack tip acceleration. It can be seen that the effect of dc/dt is more pronounced at higher crack tip accelerations.

3. Experiments

To investigate the expediency of the analysis presented in this work, a sequence of dynamic fracture experiments under mode-I conditions has been performed. In doing so, the phenomenon of transition from

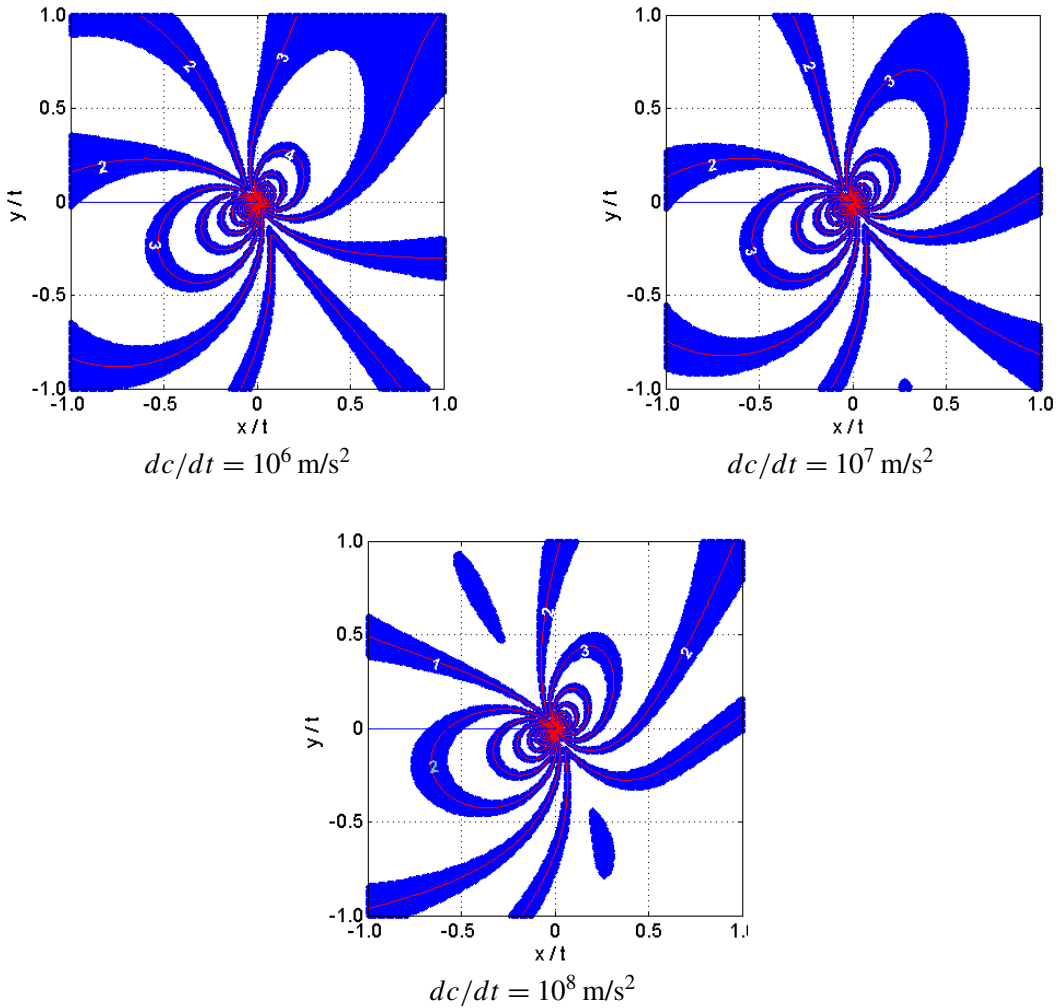


Figure 4. Effect of the crack tip acceleration on contours of the constant maximum shear stress around the crack tip in an FGM ($\alpha = 0.57$, $K_{ID}(t) = 1 \text{ MPa m}^{1/2}$, $K_{IID}(t) = 1 \text{ MPa m}^{1/2} dK_{ID}(t)/dt = 0$, $c = 650 \text{ ms}^{-1}$).

a static crack to a dynamic crack is studied. Dynamic photoelasticity along with high-speed photography is utilized to get the full field data around the crack tip during the transition.

3.1. Materials. The FGMs for this study were prepared as a particulate composite with continuously varying particle volume fraction along a single dimension. An unsaturated polyester resin (MR 17090, Ashland Chemical Company) was used as the matrix material. This highly cross-linked thermosetting polymer is ideal for fracture studies due to its relatively brittle nature. Cenospheres (LV01-SG, Sphere Services Inc.) particles with an average diameter of $127 \mu\text{m}$ were used as the filler material in the fabrication of the FGMs. These cenospheres, obtained from the fly ash of thermal power plants, are hollow spheres made of aluminum silicates.

FGM specimens were fabricated using a procedure developed in [Parameswaran and Shukla 2000]. The cenospheres have a low specific gravity of 0.67, compared to 1.18 for the resin. When the resin-cenosphere mixture is poured into the mold, the top layer of the mixture which is rich in cenospheres gets poured first and fills the bottom layer of the mold. Subsequently, the cenospheres diffuse towards the top of the mold due to buoyancy. The resin takes approximately 4 to 5 hours for gelation and once it gels and starts curing, further movement of spheres is arrested by the increased viscosity. This results in a casting with a resin rich region in the bottom, a cenosphere rich region at the top, and an intermediate region with continuously varying cenosphere content.

Detailed mechanical and physical characterization of the FGMs fabricated by the above procedure can be found in [Jain and Shukla 2004].

3.2. Specimen geometry and loading. A modified single edge notch tension (M-SENT) specimen as shown in Figure 5 is employed in this study. A first crack tip (starter crack) was made such that the subsequent crack propagation is increasing fracture toughness direction. An INSTRON 5585 apparatus is used to load the M-SENT specimens to a predetermined K_Q (static stress intensity factor) before the first crack tip is initiated by drawing a sharp knife-edge across the tip. After initiation the crack propagates across the ligament, breaking a crack detection gauge before coming to rest temporarily at the second crack tip. Breaking the crack detection gauge triggers an electronic circuit that causes the high-speed camera to commence taking a sequence of photographs of the isochromatics associated with the moving crack. At the second crack tip, the value of the stress intensity factor begins to increase

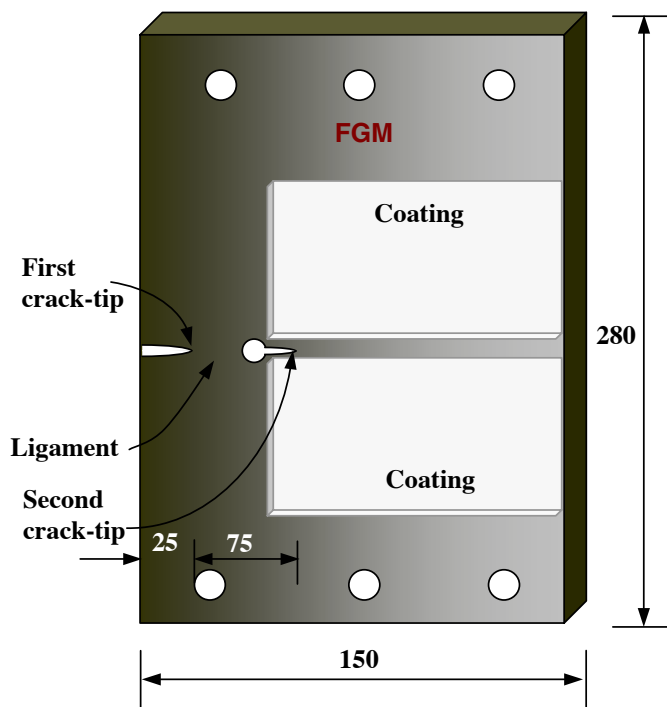


Figure 5. Specimen geometry for investigation of the transient nature of the crack tip. All dimensions are in mm.

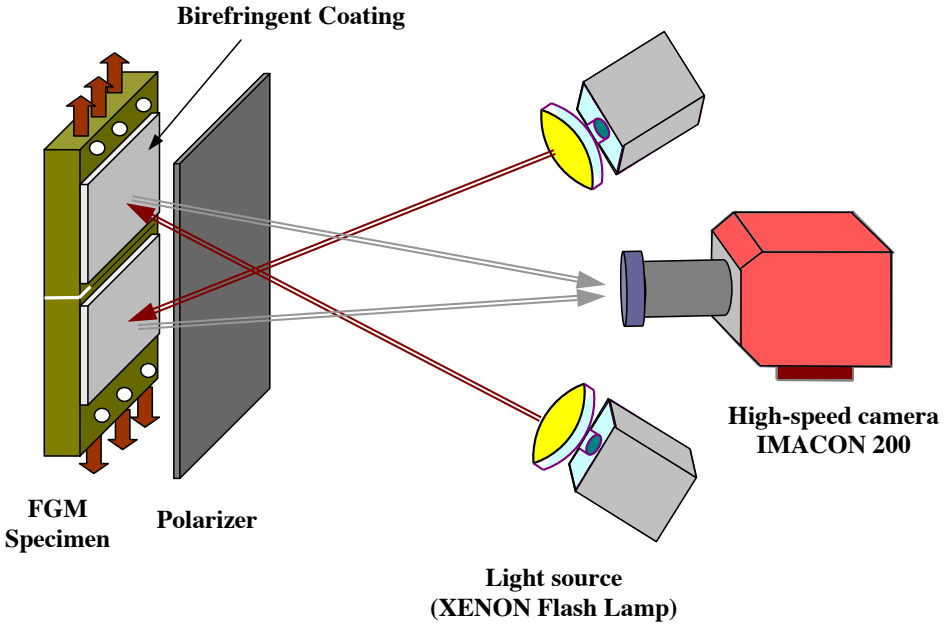


Figure 6. Photoelastic configuration for testing FGM specimens.

until it becomes sufficiently large to produce reinitiation of the crack. The bluntness of the second crack tip is controlled so that the crack remains at rest for a relatively long time (approximately $200 \mu\text{s}$) and reinitiation occurs at high values of K_Q .

3.3. Birefringent coatings. In this study we use a split birefringent coating technique [Der and Barker 1978], in which the coating is placed on both sides of the specimen, and a small distance (2 mm) away from the anticipated crack path. Birefringent coatings consisted of 3 mm thick polycarbonate sheets with vacuum deposited aluminum on the back surface. The sheets are cut to desired dimensions while using liberal amounts of cooling fluid to ensure minimum development of residual stresses. Extra fast-setting epoxy adhesive is used to bond the sheets to the specimens. Details on the validation of this technique can be found in [Jain and Shukla 2004].

3.4. High speed real time imaging of the transition from a static to a dynamic crack. A schematic of the experimental setup for testing M-SENT FGM specimens is shown in Figure 6. High speed digital imaging is employed along with dynamic photoelasticity to obtain real time, full field quantification of the transition from a static to a dynamic crack. A circular polarizer is placed in front of the split birefringent coatings to form a dark field circular polariscope. Power Light 2500DR xenon flash lamps were used as light sources to illuminate the specimen. The xenon flash lamps are a broadband source of light and therefore a monochromatic filter was placed just before the camera to ensure that the imaged isochromatic fringe patterns correspond to a single wavelength of light (546 nm). Due to stress-induced birefringence in the photoelastic coatings, this arrangement results in the formation of isochromatic fringe patterns during the failure process.

Images of the isochromatic fringes are captured using an Imacon 200 ultra-high speed digital camera. This CCD based camera provides 16 independently programmable digital images of dynamic events up to a maximum framing rate of 200×10^6 frames/s. The camera is operated with interframe times of $6 \mu\text{sec}$ (170,000 frames/sec) so as to record the increase in K at the stationary crack prior to initiation, and the dynamic value of $K(t)$ immediately after the initiation.

3.5. Photoelastic analysis. When the load is applied, the surface displacements of the specimen at the specimen-coating interface are transmitted to the coating. Observing the coating in a reflection polariscope generates a fringe pattern, which is related to the surface strains in the specimen. The method to determine the stress intensity factor is based on strain optic law applied to photoelastic coating, and on the fact that there is perfect strain transfer between specimen and coating (that is, $\varepsilon_1^S - \varepsilon_2^S = \varepsilon_1^C - \varepsilon_2^C$). We have

$$\varepsilon_1^S - \varepsilon_2^S = \varepsilon_1^C - \varepsilon_2^C = F_{CR} \frac{Nf_\varepsilon}{2hC} = F_{CR} \frac{1 + \nu^C}{EC} \frac{Nf_\sigma}{2hC}, \quad (17)$$

where f_σ is the material fringe constant associated with the incident light wave length, N is the isochromatic fringe order, h is the thickness of the coating, ν is Poisson's ratio, and superscripts S and C refer to specimen and coating, respectively.

F_{CR} is a reinforcement correction factor that accounts for the fact that the coating carries a portion of the load, causing the strain on the specimen to be reduced by a certain amount. F_{CR} essentially depends upon the relative thickness and properties of the coating and specimen [Dally and Riley 2005].

In the derivation of the crack tip fields, the FGM is assumed to be an isotropic nonhomogeneous solid, which is justified because the size of the three-dimensional zone at the crack tip (thickness/2 = 6.3 mm) is orders of magnitude larger than the cenosphere diameter (127 μm). The strain expressions obtained in Section 2.4 are substituted in (17) and the resulting equation is solved using an over-deterministic nonlinear least squares method to obtain the fracture parameters. This involves fitting of a six parameter theoretical solution, which includes K_I , K_{II} , and σ_{ox} (T -stress) and so on, to field data taken from the isochromatic loops.

4. Experimental results

A series of experiments were conducted with K_Q ranging from 1.0 to 1.25 MPa m^{1/2}. Figure 7 shows a set of six frames recorded during the transition from a static to a dynamic crack. Isochromatics from each of the frames are analyzed using the aforementioned photoelastic procedure to obtain the stress intensity factor history. The crack remains stationary until frame 6 and starts moving afterwards. The size of the isochromatics decreases substantially as soon as the second crack starts to move, indicating the reduction in the value of stress intensity factor around the crack tip. These isochromatics are analyzed using the procedure described in the previous sections to obtain the dynamic stress intensity factor. The photoelastic fringes were regenerated using the calculated fracture parameters from data analysis. A good agreement between the regenerated fringes and the experimental fringes were observed.

Figure 8 shows the extension of the second crack with time. Measurements were repeated five times and the 95% confidence interval obtained using the Student's t -distribution is also shown. As the crack starts to move, the velocity of the crack continuously increases until it reaches a certain value and then stays constant. The crack initiation time is estimated to be 26.1 μsec , from curve fitting.

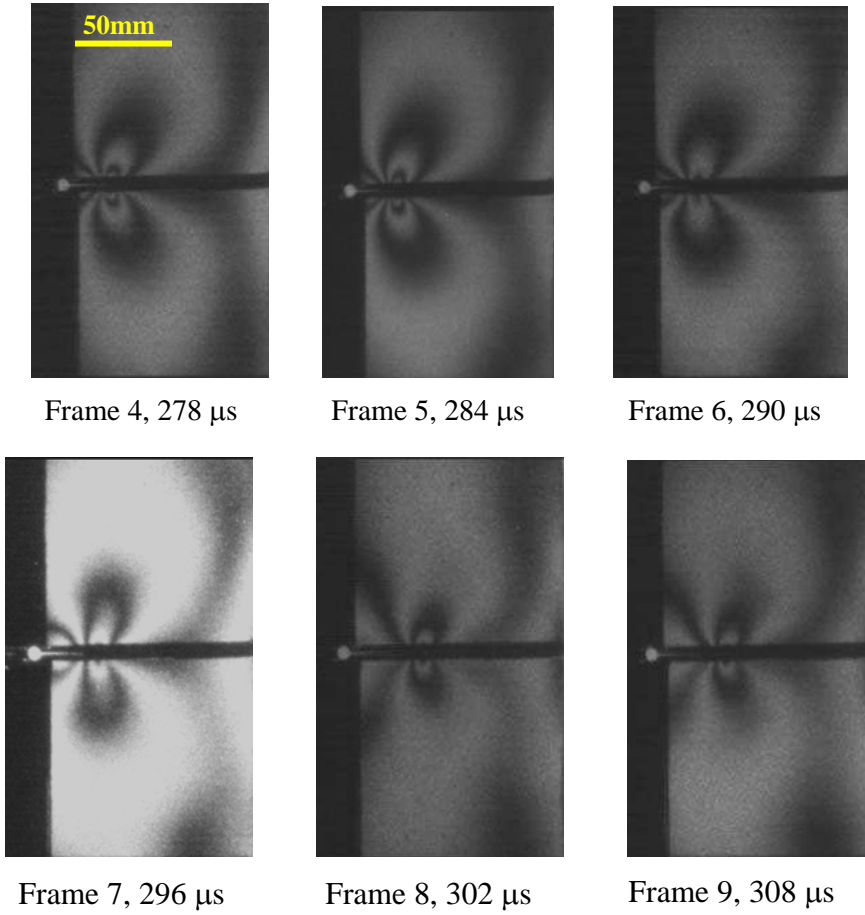


Figure 7. Isochromatic fringe patterns during crack initiation at a second crack tip.

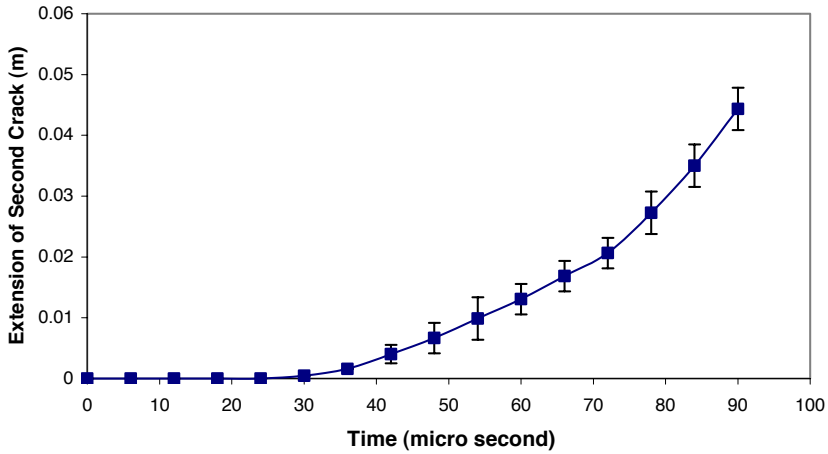


Figure 8. Crack tip position as a function of time.

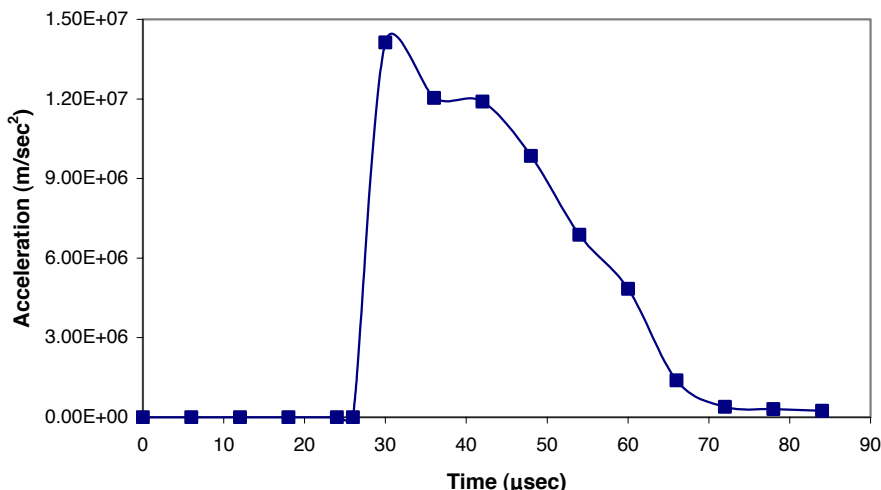


Figure 9. Crack tip acceleration as a function of time.

The crack propagation profile and time of initiation are subsequently used for calculating crack acceleration. The acceleration profile is plotted in Figure 9 and shows that crack acceleration is 1.4×10^7 m/sec² just after initiation and decreases afterwards. It is plausible that crack acceleration is even higher as crack extension occurs by void coalescence and the crack jumps from zero to finite velocity.

Figure 10 shows the variation of the stress intensity factor with time. The stress intensity factor increases monotonically at the arrested crack until K_Q becomes large enough to produce initiation at the second crack tip. The first frame was captured after $4 \mu\text{sec}$, which is approximately the time for the shear wave to clear the near field region ($r = 5$ mm). It can be seen that the stress intensity factor decreases rapidly from $K_Q = 1.38 \text{ MPa m}^{1/2}$ to $K(t) = 0.97 \text{ MPa m}^{1/2}$ in $4 \mu\text{sec}$. The stress intensity factor decreases further to $0.88 \text{ MPa m}^{1/2}$ after which it shows monotonic increase.

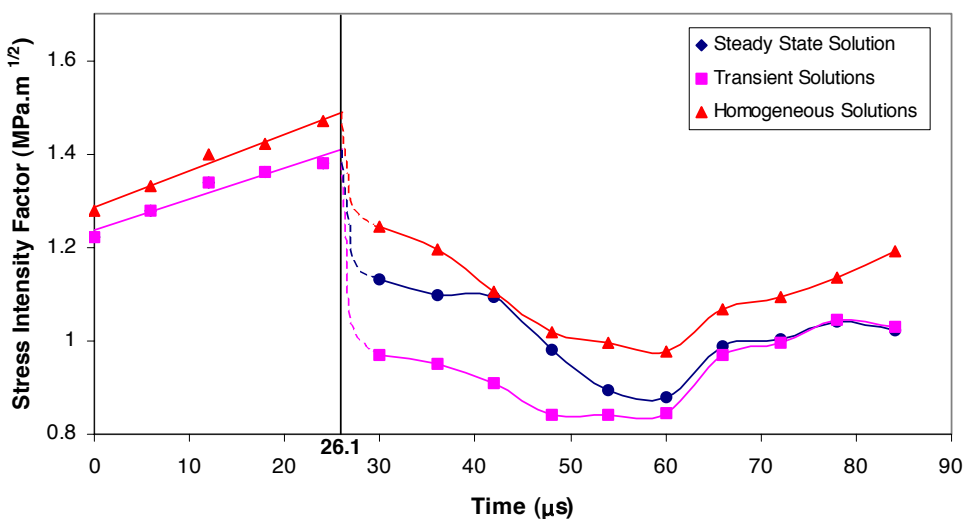


Figure 10. Stress intensity factor as a function of time.

To investigate the effect of transient higher order terms, analysis is also performed neglecting the transient higher order terms. The stress intensity factor history thus obtained using the steady state solution is also shown in Figure 10. The average error introduced by neglecting transient higher order terms is as high as 20%. It is also observed that after 60 μ sec, when the crack tip acceleration decreases considerably, the instantaneous stress intensity factor obtained with transient fields and steady state fields are in good agreement. This suggests that it is essential to include transient higher order terms in the stress field expansion in order to obtain an accurate value of the instantaneous stress intensity factor during highly transient phenomena.

Figure 10 also shows the stress intensity factor history obtained using just the homogeneous stress field expansion. As expected, the error induced by just using homogeneous terms for analyzing the isochromatics in FGMs can be as high as 30% in the estimation of the stress intensity factor.

5. Concluding remarks

Motivated by the transient nature of the elastic fields in the vicinity of a growing crack tip, an approximation of the near-tip field in the form of an asymptotic expansion has been introduced. The analysis is performed for a crack growing in an arbitrary direction in an FGM. The higher order terms in the expansions take into account the recent history of the stress intensity factor and crack motion. The solution thus obtained is used to examine the effect of the transient terms on the near-tip stress fields. This is accomplished by discussing the effect of crack tip acceleration and rate of change of the stress intensity factor on synthetically generated contours of constant maximum shear stress and constant first stress invariant. To investigate the expediency of the analysis presented in this work, a sequence of dynamic fracture experiments has been performed. In doing so, the phenomenon of transition from a static crack to a dynamic crack is utilized. It is found that during this transition the crack tip accelerations can be as high as 10^8 m/sec². The full field data obtained from these transition experiments were analyzed using the analytically derived equations. It is found that not including the transient higher order terms in the stress field expansion during highly transient phenomena might give rise to errors as high as 20% in the estimation of the stress intensity factor.

Appendix: Coefficients occurring in the expressions of ϕ_2 and ψ_2 , pages 600–601.

$$\begin{aligned}
 D_I(A_0(t)) &= -\frac{3c^{1/2}\rho_0}{\alpha_l^2\mu_0(k+2)}\frac{d}{dt}(c^{1/2}A_0(t)) & B_l^A(t) &= \frac{3c^2}{2\alpha_l^4}\left(\frac{\rho_0}{\mu_0(k+2)}\right)^2 A_0(t)\frac{dc}{dt} \\
 D_I(C_0(t)) &= -\frac{3c^{1/2}\rho_0}{\alpha_l^2\mu_0(k+2)}\frac{d}{dt}(c^{1/2}C_0(t)) & B_l^C(t) &= \frac{3c^2}{2\alpha_l^4}\left(\frac{\rho_0}{\mu_0(k+2)}\right)^2 C_0(t)\frac{dc}{dt} \\
 D_s(B_0(t)) &= -\frac{3c^{1/2}\rho_0}{\alpha_s^2\mu_0}\frac{d}{dt}(c^{1/2}B_0(t)) & B_s^B(t) &= \frac{3c^2}{2\alpha_s^4}\left(\frac{\rho_0}{\mu_0}\right)^2 B_0(t)\frac{dc}{dt} \\
 D_s(D_0(t)) &= -\frac{3c^{1/2}\rho_0}{\alpha_s^2\mu_0}\frac{d}{dt}(c^{1/2}D_0(t)) & B_s^D(t) &= \frac{3c^2}{2\alpha_s^4}\left(\frac{\rho_0}{\mu_0}\right)^2 D_0(t)\frac{dc}{dt}
 \end{aligned}$$

References

- [Abanto-Bueno and Lambros 2006] J. Abanto-Bueno and J. Lambros, “An experimental study of mixed mode crack initiation and growth in functionally graded materials”, *Exp. Mech.* **46**:2 (2006), 179–196.
- [Atkinson and List 1978] C. Atkinson and R. D. List, “Steady state crack propagation into media with spatially varying elastic properties”, *Int. J. Eng. Sci.* **16**:10 (1978), 717–730.
- [Chalivendra et al. 2003] V. B. Chalivendra, A. Shukla, and V. Parameswaran, “Quasi-static stress fields for a crack inclined to the property gradation in functionally graded materials”, *Acta Mech.* **162**:1-4 (2003), 167–184.
- [Dally and Riley 2005] J. W. Dally and W. F. Riley, *Experimental stress analysis*, College House Enterprises, 2005.
- [Dally and Shukla 1979] J. W. Dally and A. Shukla, “Dynamic crack behavior at initiation”, *Mech. Res. Commun.* **6**:4 (1979), 239–244.
- [Der and Barker 1978] V. K. Der and D. C. Barker, D. B. and Holloway, “A split birefringent coating technique to determine dynamic stress intensity factors”, *Mech. Res. Commun.* **5**:6 (1978), 313–318.
- [Erdogan 1995] F. Erdogan, “Fracture mechanics of functionally graded materials”, *Compos. Eng.* **5**:7 (1995), 753–770.
- [Freund 1990] L. B. Freund, *Dynamic fracture mechanics*, Cambridge University Press, Cambridge, 1990.
- [Freund and Rosakis 1992] L. B. Freund and A. J. Rosakis, “The structure of the near-tip field during transient elastodynamic crack growth”, *J. Mech. Phys. Solids* **40**:3 (1992), 699–719.
- [Gu and Asaro 1997] P. Gu and R. J. Asaro, “Cracks in functionally graded materials”, *Int. J. Solids Struct.* **34**:1 (1997), 1–17.
- [Jain and Shukla 2004] N. Jain and A. Shukla, “Displacements, strains and stresses associated with propagating cracks in materials with continuously varying properties”, *Acta Mech.* **171**:1-2 (2004), 75–103.
- [Jain and Shukla 2006] N. Jain and A. Shukla, “Mixed mode dynamic fracture in particulate reinforced functionally graded materials”, *Exp. Mech.* **46**:2 (2006), 137–154.
- [Jain et al. 2004] N. Jain, C. E. Rousseau, and A. Shukla, “Crack-tip stress fields in functionally graded materials with linearly varying properties”, *Theor. Appl. Fract. Mech.* **42**:2 (2004), 155–170.
- [Jin and Noda 1994] Z. H. Jin and N. Noda, “Crack-tip singular field in nonhomogeneous materials”, *J. Appl. Mech. (Trans. ASME)* **61** (1994), 738–739.
- [Kim and Paulino 2004] J. H. Kim and G. H. Paulino, “ T -stress in orthotropic functionally graded materials: Lekhnitskii and Stroh formalisms”, *Int. J. Fract.* **126**:4 (2004), 345–384.
- [Li and Weng 2002] C. Y. Li and G. J. Weng, “Yoffe-type moving crack in a functionally graded piezoelectric material”, *P. Roy. Soc. Lond. A Mat.* **A458**:2018 (2002), 381–399.
- [Li et al. 2000] H. Li, J. Lambros, B. A. Cheeseman, and M. H. Santare, “Experimental investigation of the quasi-static fracture of functionally graded materials”, *Int. J. Solids Struct.* **37**:27 (2000), 3715–3732.
- [Marur and Tippur 2000] P. R. Marur and H. V. Tippur, “Numerical analysis of crack tip fields in functionally graded materials with a crack normal to the elastic gradient”, *Int. J. Solids Struct.* **37**:38 (2000), 5353–5370.
- [Nakagaki et al. 1998] M. Nakagaki, H. Sasaki, and S. Hagihara, “A study of crack in functionally graded material under dynamic loading”, *Dynamic Fracture, Failure and Deformation, ASME* **300** (1998), 1–6.
- [Parameswaran and Shukla 1998] V. Parameswaran and A. Shukla, “Dynamic fracture of a functionally gradient material having discrete property variation”, *J. Mater. Sci.* **33**:13 (1998), 3303–3311.
- [Parameswaran and Shukla 2000] V. Parameswaran and A. Shukla, “Processing and characterization of a model functionally gradient materials”, *J. Mater. Sci.* **35**:1 (2000), 21–29.
- [Rousseau and Tippur 2001] C.-E. Rousseau and H. V. Tippur, “Dynamic fracture of compositionally graded materials with cracks along the elastic gradient: experiments and analysis”, *Mech. Mater.* **33**:7 (2001), 403–421.
- [Shukla and Chona 1987] A. Shukla and R. Chona, “The stress field surrounding a rapidly propagating curving crack”, pp. 86–99 in *Fracture Mechanics: Eighteenth Symposium, ASTM STP 945*, edited by D. T. Read and R. P. Reed, 1987.
- [Shukla and Jain 2004] A. Shukla and N. Jain, “Dynamic damage growth in particle reinforced graded materials”, *Int. J. Impact Eng.* **30**:7 (2004), 777–803.

- [Sladek et al. 2005] J. Sladek, V. Sladek, and C. Zhang, “The MLPG method for crack analysis in anisotropic functionally graded materials”, *Structure Integrity and Durability* **1** (2005), 131–144.
- [Surendranath et al. 2003] H. Surendranath, H. A. Bruck, and S. Gowrisankaran, “Enhancing the optimization of material distributions in composite structures using gradient architectures”, *Int. J. Solids Struct.* **40**:12 (2003), 2999–3020.
- [Suresh and Mortensen 1998] S. Suresh and A. Mortensen, *Functionally graded materials*, The Institute of Materials, IOM Communications Ltd., London, 1998.
- [Tilbrook et al. 2005] M. T. Tilbrook, R. J. Moon, and M. Hoffman, “Curved crack propagation in homogeneous and graded materials”, *Fatigue Fract. Eng. Mater. Struct.* **28**:11 (2005), 939–950.
- [Wang and Meguid 1994] X. D. Wang and S. A. Meguid, “On the dynamic crack propagation in an interface with spatially varying elastic properties”, *Int. J. Fract.* **69**:1 (1994), 87–99.
- [Zhang et al. 2003] C. Zhang, J. Sladek, and V. Sladek, “Effects of material gradients on transient dynamic mode-III stress intensity factors in a FGM”, *Int. J. Solids Struct.* **40**:20 (2003), 5251–5270.

Received 27 Jul 2006. Accepted 23 Sep 2006.

NITESH JAIN: nitesh_jain@goodyear.com

Corporate Research, The Goodyear Tire and Rubber Company, 142 Goodyear Blvd., Akron, OH 44305, United States

ARUN SHUKLA: shuklaa@egr.uri.edu

Dynamic Photomechanics Laboratory, Department of Mechanical Engineering and Applied Mechanics, University of Rhode Island, 110 Wales Hall, 92 Upper College Rd., Kingston, RI 02881, United States